The Astrophysical Journal Letters, 889:L36 (6pp), 2020 February 1 https://doi.org/10.3847/2041-8213/ab6ddc

Identification of QPO Frequency of GRS 1915+105 as the Relativistic Dynamic Frequency of a Truncated Accretion Disk

Ranjeev Misra[1], Divya Rawat[2], J S Yadav[2], and Pankaj Jain[2]
[1] Inter-University Center for Astronomy and Astrophysics, Ganeshkhind, Pune 411007, India
[2] Department of physics, IIT Kanpur, Kanpur, Uttar Pradesh 208016, India; divyar@iitk.ac.in
Received 2019 October 12; revised 2020 January 18; accepted 2020 January 20; published 2020 February 3

Abstract

We have analyzed *AstroSat* observations of the galactic microquasar system GRS 1915+105, when the system exhibited C-type quasi-periodic oscillations (QPOs) in the frequency range of 3.4–5.4 Hz. The broadband spectra (1–50 keV) obtained simultaneously from the Large Area X-ray Proportional Counter and Soft X-ray Telescope can be well described by a dominant relativistic truncated accretion disk along with thermal Comptonization and reflection. We find that while the QPO frequency depends on the inner radii with a large scatter, a much tighter correlation is obtained when both the inner radii and accretion rate of the disk are taken into account. In fact, the frequency varies just as the dynamic frequency (i.e., the inverse of the sound crossing time) does as predicted decades ago by the relativistic standard accretion disk theory for a black hole with a spin parameter of ∼0.9. We show that this identification has been possible due to the simultaneous broadband spectral coverage with temporal information as obtained from *AstroSat*.

Unified Astronomy Thesaurus concepts: Accretion (14); Stellar mass black holes (1611); Rotating black holes (1406); Astrophysical black holes (98); Low-mass x-ray binary stars (939); Black hole physics (159); Kerr black holes (886); Relativistic disks (1388); A stars (5); Relativity (1393); X-ray astronomy (1810)

1. Introduction

For a test particle orbiting a black hole, there are three characteristic frequencies depending on the radius (Stella et al. 1999a, 1999b). The first is the Keplerian frequency that is the inverse of the time period of the orbit. There is the periastron precession frequency that is the Keplerian frequency minus the Epicyclic one and relates to how an orbit will precess in General Relativity. There is also the Lense–Thirring precession frequency, which is related to the wobbling of the orbit out of the plane that arises only in General Relativity when the black hole is spinning.

Apart from these three relativistic test particle frequencies, there are two other frequencies related to the two characteristic speeds in an accretion disk, the sound ($c_s(r)$) and the radial inflow speeds ($v_r(r)$), where r is the radial distance. The dynamical frequency is the inverse of the sound crossing time, i.e., $f_{\rm dyn} \sim c_s(r)/r$. In the standard thin relativistic accretion disk (Novikov & Thorne 1973; Shakura & Sunyaev 1973) the sound speed is

$$c_s(r) = h(r)(GM/r^3)^{1/2} A^{-1} B^{1} C^{-1/2} D^{1/2} E^{1/2}, \quad (1)$$

where M is the mass of the black hole. The relativistic terms A, B, C, D, and E are functions of r and the black hole spin parameter, a. They asymptotically tend to unity in the Newtonian limit, i.e., when r tends to infinity. The scale height in the inner regions of the disk is given by

$$h(r, a) \sim 10^6 {\rm cm}\ \ \dot{M}_{18} A^2 B^{-3} C^{1/2} D^{-1} E^{-1} L, \quad (2)$$

where $\dot{M}_{18}$ is the accretion rate in units of 10^{18} grams s^{-1}. The relativistic term L is a function of r and a and arises due to the relativistic phenomenon of the existence of a last stable orbit at which the disk flow no longer depends on viscosity and the height vanishes. Thus,

$$\frac{f_{\rm dyn}}{\dot{M}_{18}} = N\ 8979\ {\rm Hz}\ (r/r_g)^{-2.5}\ (M/12.4M_\odot)^{-2} \times A^{1} B^{-2} D^{-0.5} E^{-0.5} L, \quad (3)$$

where $r_g = GM/c^2$ is the gravitational radius and the mass of the black hole, M has been scaled by $12.4M_\odot$, which is the reported black hole mass for the source GRS 1915+105 (Reid et al. 2014). N is a factor of order unity to incorporate the assumptions made in the standard accretion disk theory especially in the radiative transfer equation. It should be emphasized that A, B, D, E, and L are functions of radii and are important for small radii, $r < 10r_g$. Thus, the functional form of $f_{\rm dyn}$ significantly deviates from its Newtonian dependence of $\propto r^{-2.5}$ in this regime. Note that $f_{\rm dyn}$ does not depend on the unknown turbulent viscosity parameter α of the standard disk theory in contrast to the viscous timescale $\tau_{\rm visc} \sim r/v_r$, where v_r is the radial inflow velocity of the disk. $\tau_{\rm visc}$ is an order of magnitude higher than the dynamical timescale and depends inversely on both α and the accretion rate squared.

X-ray binaries show variability on a wide range of timescales which include broadband noise and nearly periodic oscillations termed as quasi-periodic oscillations (QPOs; van der Klis 2005). For systems harboring black holes, the QPO frequency ranges from milli-Hertz to hundreds of Hertz prompting classification in very low (milli-Hz), low (Hz), and high frequency QPOs (∼100 Hz). Low-frequency QPOs occur at different spectral states and have been further classified as A-, B-, and C-type QPOs (Wijnands et al. 1999; Homan et al. 2001; Remillard et al. 2002; Casella et al. 2004). This multitude of QPOs suggested that they perhaps correspond to different characteristic timescales of the system described above. Moreover, since the frequency of a particular type of QPO

varies, the radius responsible for the phenomenon should also be varying. An attractive candidate for this radius is the truncation or inner radius of a standard disk beyond which there is a hot inner flow (Shapiro et al. 1976; Narayan & McClintock 2008). Since the characteristic timescales depend on General Relativistic corrections, identification of a QPO frequency with one, opens the exciting possibility of testing the theory in the strong field regime.

However, as discussed below it has proved to be difficult to make reliable and independent estimates of the inner disk radius. Indirect schemes have been employed to identify the QPO frequencies. For example, taking advantage of the different radial dependencies of the characteristic frequencies, correlation between frequencies of different QPOs, or breaks in the broadband noise have been used to identify the QPO frequencies (Psaltis et al. 1999; Stella et al. 1999a, 1999b; Belloni et al. 2002). This method depends on the relatively rare detection of more than two QPOs at the same time (Motta et al. 2014). Another method has been to use the correlation of the QPO frequency with some other features, such as the high-energy spectral index, as a proxy for a characteristic radius (Titarchuk & Osherovich 1999). However, since the dependence of the high-energy spectral index on radius is model dependent and sensitive to assumptions of the unknown viscosity, the best one can obtain are empirical scaling relations, which have proved useful to compare between different black hole systems (Titarchuk & Fiorito 2004).

The inner radius of an accretion disk can be measured by fitting the spectra of these sources with a truncated accretion disk model (Muno et al. 1999; Sobczak et al. 2000). Until recently, the detection of QPOs in black hole systems has been done by the Proportional Counter Array (PCA) on board the *Rossi X-ray Timing Experiment* (*RXTE*) observatory. Since the radius has to be measured strictly simultaneously with the QPO, the spectral analysis needed to be restricted to data obtained from *RXTE*. However, the PCA had a relatively poor spectral resolution and its effective energy range was from 3 to 20 keV, while the typical maximum color temperature of the disk is around 1 keV. Moreover, since the spectral data were restricted in the energy range, simple models had to be used to fit the spectra. This limited energy range led to severe systematic uncertainties in the inner disk radius with some values being unphysically small. Moreover, the results were sometimes contradictory like QPO frequency increasing with radius for one system while decreasing for another (Sobczak et al. 2000). Nevertheless, correlations have been observed between the frequency and the radius that have been used as evidence for some models, although there were large scatter in the estimated values (Mikles et al. 2009). A critical limitation of these earlier works was that these analyses were not sensitive enough to test the variation of the QPO frequency with accretion rate, since that requires broadband data.

The Large Area X-ray Proportional Counter (LAXPC; Yadav et al. 2016; Agrawal et al. 2017) and the Soft X-ray Telescope (SXT; Singh et al. 2016, 2017) on board the Indian Space Observatory *AstroSat* (Agrawal 2017) are ideally suited to study correlation between the QPO frequency and the disk inner radius. The high time precision and the large area of LAXPC provide timing and spectral information in the 4–50 keV band; the SXT provides simultaneous spectral coverage in the low 1.0–5.0 keV band. As reported by Rawat et al. (2019), *AstroSat* observed the black hole system GRS 1915+105 from 2017 March 28 18:03:19 until 2017 March 29 19:54:07 when the source transited from a relatively steady state called χ class, through an intermediate state (IMS), to a flaring state (heartbeat state (HS)) where large amplitude oscillations are seen. All through the observation, the source exhibited C-type QPOs in the frequency range 3.4–5.4 Hz.

In this work, we examine the spectral evolution of the source during this observation and supplement the results with observations made two days later on 2017 April 1, when the source shows both χ and HS with QPOs in the same frequency range. It was fortuitous that the source was undergoing a transition and showed a QPO all throughout enabling us to study the spectral properties of the source and correlate them with the varying QPO frequency.

2. Data Analysis

2.1. Timing Analysis

Rawat et al. (2019) split the 2017 March 28 observation into several segments and presented the timing properties for each of them. From the power density spectra (PDSs) they obtained the QPO frequencies for segments corresponding to the χ, intermediate, and HS. Following Rawat et al. (2019) we do the same analysis for the *AstroSat* LAXPC observation of GRS 1915+105 during 2017 April 1 00:03:21 until April 1 14:38:01. The data were analyzed for the two units LAXPC 10 and LAXPC 20, using LaxpcSoft.[3] Like the earlier observation, the source exhibited χ and HSs that were divided into six segments (two for χ and four for the HS). Lightcurves for representative segments for a χ and HS are shown in the top panel of Figure 1 and the corresponding PDSs are shown in the bottom panel. The PDSs were fitted using Lorentzian functions, and the QPO frequency with error was estimated using the same technique given in Rawat et al. (2019). Thus, combining the two observations we have a total of 16 segments (5 for χ, 3 for intermediate, and 8 for the HSs) for which the QPO frequency has been estimated and tabulated in the first column of Table 1.

2.2. Spectral Analysis

For each of the 16 segments, simultaneous spectral data were obtained from LAXPC 10, 20, and SXT. The LAXPC spectra, background, and response files were generated using LaxpcSoft (see footnote 3). For SXT data reduction recent arf and rmf files are used, details of which are given at the *AstroSat* website.[4] The SXT spectra were extracted from a source region of 12′, and the standard background spectra were used for all spectra.

The SXT (energy range 1.0–5.0 keV) and LAXPC 10 and 20 (energy range 4–50 keV) spectra of each data set were analyzed together using the X-ray spectra fitting software XSPEC (Arnaud 1996) using its inbuilt models. During the spectral fitting, gain variation for SXT was taken into account by using the gain fit command in XSPEC. The offset value obtained ranged from 1.4 to 2.4 eV. An additional systematic error of 3% was included. To take into account possible uncertainties in the effective area of the instruments a variable constant was included for the LAXPC 10 and 20 spectra relative to SXT, whose values ranged from 0.81 to 0.92.

The spectra were fitted using the relativistic disk model "kerrd" (Ebisawa et al. 2003) and the convolution model "simpl" (Steiner et al. 2009) to take into account the Comptonization of

[3] http://astrosat-ssc.iucaa.in/?q=laxpcData
[4] http://astrosat-ssc.iucaa.in/?q=sxtData

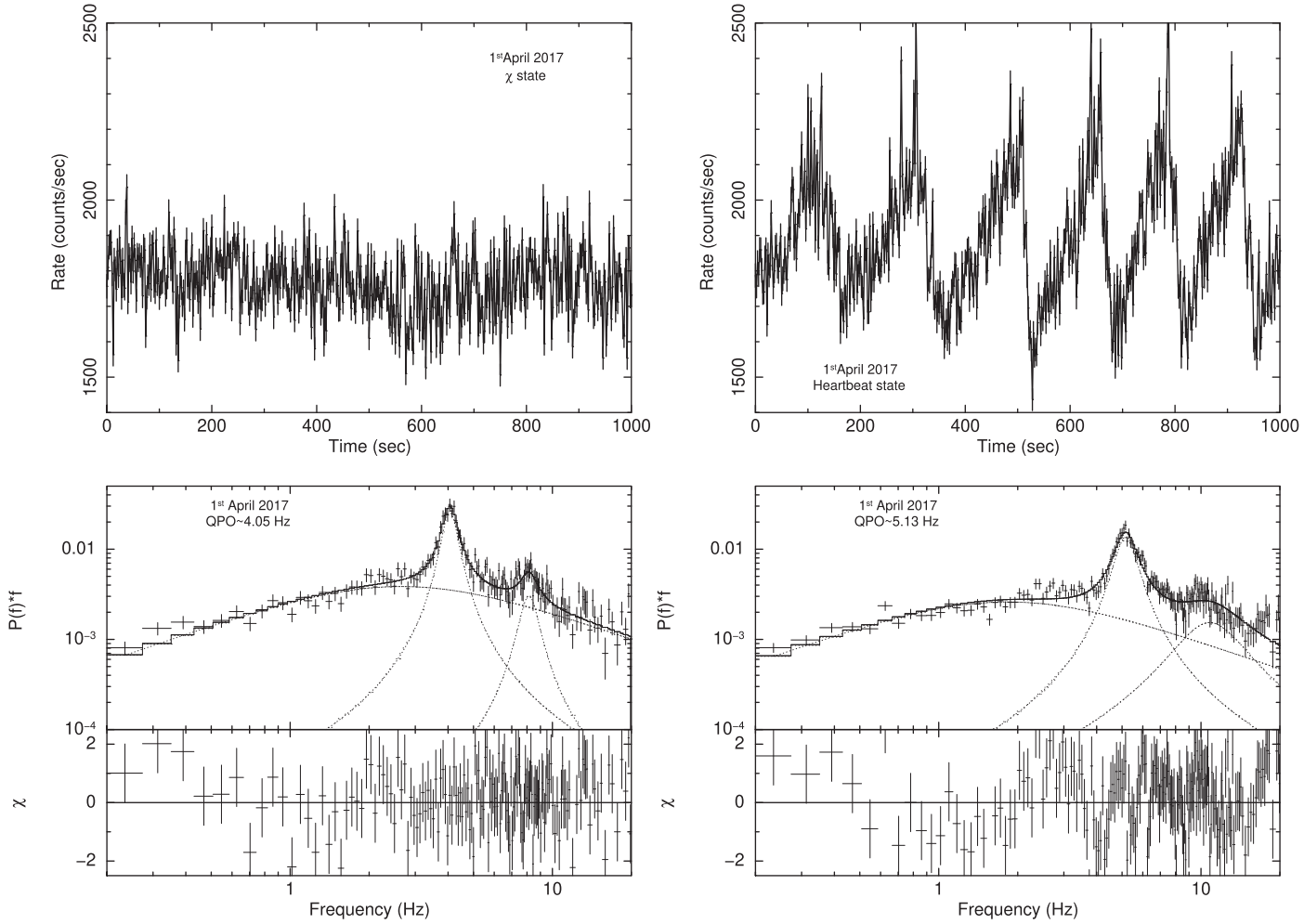

Figure 1. Top panel shows the 2.0 s binned 1000 s lightcurves of χ class and HS. The corresponding PDSs in the 0.2–20.0 Hz range are shown in the bottom panels. LAXPC10 and LAXPC20 are used for lightcurve and PDS extraction here.

Table 1
Spectral Parameters for GRS 1915+105 in the 1.0–50.0 keV Energy Range

Exposure Time (s)	State	QPO Frequency (Hz)	Accretion Rate (10^{18} gm s^{-1})	Inner Radius (R_g)	Fraction Scatter	Gamma	Flux in Line Emission (10^{-2} photons cm^{-2} s^{-1})	χ^2/Dof
			2017 March 28th					
1199	χ class	$3.59^{+0.01}_{-0.01}$	$0.67^{+0.01}_{-0.02}$	$4.62^{+0.15}_{-0.06}$	$0.42^{+0.01}_{-0.01}$	$2.169^{+0.005}_{-0.005}$	$1.1^{+0.2}_{-0.1}$	488.7/426
1199	χ class	$3.46^{+0.02}_{-0.02}$	$0.74^{+0.04}_{-0.03}$	$5.25^{+0.27}_{-0.24}$	$0.43^{+0.02}_{-0.02}$	$2.169^{+0.011}_{-0.005}$	$1.1^{+0.2}_{-0.2}$	492.1/424
1203	χ class	$3.65^{+0.01}_{-0.02}$	$0.77^{+0.03}_{-0.03}$	$5.31^{+0.19}_{-0.15}$	$0.45^{+0.02}_{-0.01}$	$2.221^{+0.006}_{-0.007}$	$1.0^{+0.2}_{-0.2}$	509.4/431
903	IMS	$4.08^{+0.03}_{-0.02}$	$0.71^{+0.03}_{-0.04}$	$4.20^{+0.20}_{-0.29}$	$0.39^{+0.01}_{-0.01}$	$2.223^{+0.009}_{-0.011}$	$0.9^{+0.3}_{-0.2}$	489.4/411
477	IMS	$4.17^{+0.03}_{-0.03}$	$0.74^{+0.04}_{-0.04}$	$4.53^{+0.25}_{-0.30}$	$0.40^{+0.02}_{-0.01}$	$2.247^{+0.012}_{-0.013}$	$0.9^{+0.3}_{-0.3}$	298.8/322
840	IMS	$4.38^{+0.07}_{-0.06}$	$0.68^{+0.02}_{-0.04}$	$3.58^{+0.17}_{-0.27}$	$0.35^{+0.01}_{-0.01}$	$2.260^{+0.013}_{-0.014}$	⋯	419.1/410
1209	HS	$5.08^{+0.04}_{-0.03}$	$0.65^{+0.01}_{-0.03}$	$3.02^{+0.09}_{-0.24}$	$0.29^{+0.01}_{-0.01}$	$2.255^{+0.014}_{-0.017}$	⋯	519.6/437
1211	HS	$5.15^{+0.03}_{-0.03}$	$0.64^{+0.03}_{-0.00}$	$2.90^{+0.18}_{-0.03}$	$0.29^{+0.01}_{-0.01}$	$2.241^{+0.014}_{-0.009}$	⋯	492.7/436
1213	HS	$5.33^{+0.03}_{-0.03}$	$0.66^{+0.02}_{-0.02}$	$2.80^{+0.12}_{-0.09}$	$0.27^{+0.01}_{-0.01}$	$2.239^{+0.012}_{-0.006}$	⋯	539.4/439
1216	HS	$5.42^{+0.03}_{-0.03}$	$0.69^{+0.01}_{-0.01}$	$3.03^{+0.09}_{-0.14}$	$0.26^{+0.01}_{-0.01}$	$2.252^{+0.012}_{-0.007}$	⋯	490.5/437
			2017 April 1st					
634	χ class	$4.05^{+0.02}_{-0.02}$	$0.78^{+0.04}_{-0.04}$	$4.84^{+0.32}_{-0.31}$	$0.38^{+0.01}_{-0.01}$	$2.219^{+0.012}_{-0.012}$	$1.0^{+0.2}_{-0.2}$	347.2/374
204	χ class	$4.67^{+0.04}_{-0.04}$	$0.79^{+0.06}_{-0.07}$	$4.42^{+0.35}_{-0.47}$	$0.36^{+0.01}_{-0.01}$	$2.274^{+0.017}_{-0.020}$	$0.7^{+0.4}_{-0.2}$	222.3/199
748	HS	$5.13^{+0.03}_{-0.03}$	$0.72^{+0.02}_{-0.02}$	$3.44^{+0.12}_{-0.20}$	$0.31^{+0.00}_{-0.00}$	$2.278^{+0.003}_{-0.003}$	⋯	438.1/407
1175	HS	$5.13^{+0.02}_{-0.02}$	$0.71^{+0.02}_{-0.03}$	$3.27^{+0.13}_{-0.17}$	$0.31^{+0.01}_{-0.01}$	$2.287^{+0.015}_{-0.014}$	⋯	519.5/439
1260	HS	$5.12^{+0.01}_{-0.01}$	$0.72^{+0.02}_{-0.02}$	$3.44^{+0.14}_{-0.13}$	$0.30^{+0.01}_{-0.01}$	$2.262^{+0.013}_{-0.013}$	⋯	458.9/439
762	HS	$5.27^{+0.04}_{-0.04}$	$0.69^{+0.04}_{-0.01}$	$3.09^{+0.22}_{-0.10}$	$0.28^{+0.01}_{-0.01}$	$2.245^{+0.014}_{-0.014}$	⋯	459.4/411

Note. Here, IMS and HS stand for intermediate and heartbeat states respectively.

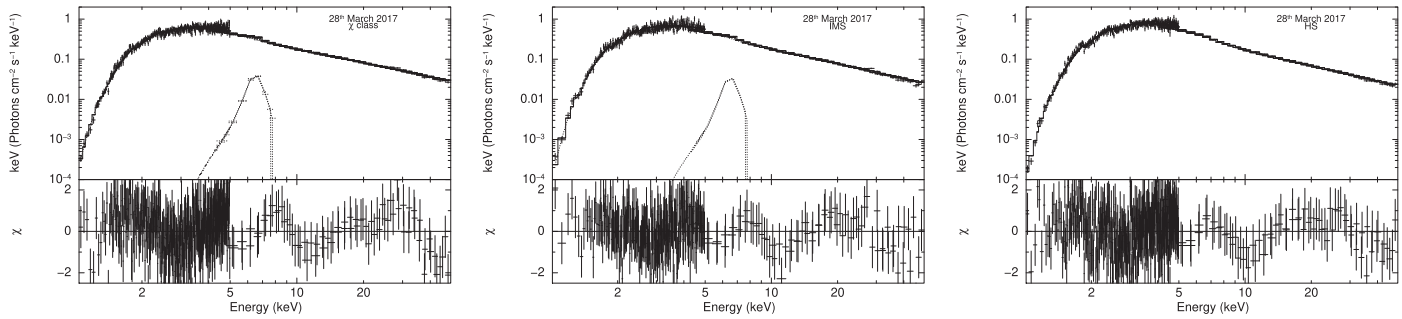

Figure 2. Spectral fitting including residuals are shown for χ state, IMS, and HS.

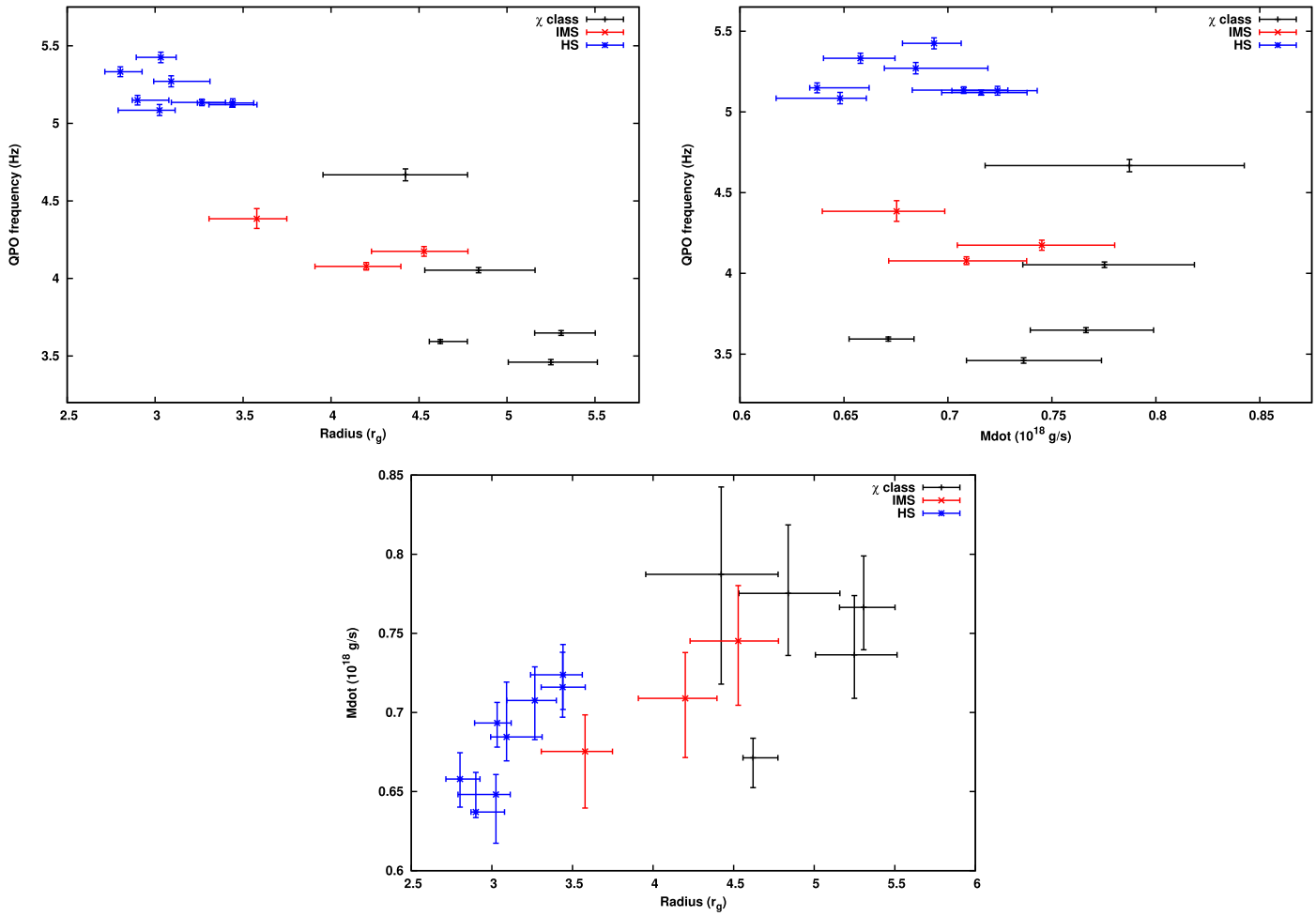

Figure 3. Variation of QPO frequencies with inner disk radii and accretion rate are shown in the upper left and upper right panels, respectively. The bottom panel shows the variation of the accretion rate with inner disk radii.

the disk photons in the inner flow. The accretion rate and the inner radius of the disk were estimated from the best-fit values obtained from the "kerrd" model. The mass of the black hole, distance to the source, and inclination angle of the disk were taken to be $12.4 M_{\odot}$, 8.6 kpc, and 60° (Reid et al. 2014), respectively. The color factor was fixed to 1.7 (Shimura & Takahara 1995).

To take into account a relativistically smeared iron fluorescence line, the model "kerrdisk" (Brenneman & Reynolds 2006) was used. While the "kerrd" model implicitly assumes a fast spinning black hole, the spin is a parameter for "kerrdisk" that was fixed at 0.98 (Blum et al. 2009), as the spectral fitting was found to be insensitive to its value. For the kerrdisk the emissivity index for both the inner and outer parts of the disk was fixed at 1.8 (Blum et al. 2009). The rest-frame energy of the iron line was fixed at 6.4 keV (Blum et al. 2009). The inner radius was tied to that used for the "kerrd" after dividing by an appropriate factor of 1.235, since for "kerrd," the radius is measured in r_g, while for the kerrdisk it is in units of the radius of marginal stability. Absorption by intervening matter was modeled using "tbabs" (Wilms et al. 2000) with a column density fixed at $4 \times 10^{22}\,\mathrm{cm}^{-2}$ (Blum et al. 2009). Representative spectra for a χ, intermediate, and HS are shown in Figure 2. Note that for the spectra of HS the iron line component is

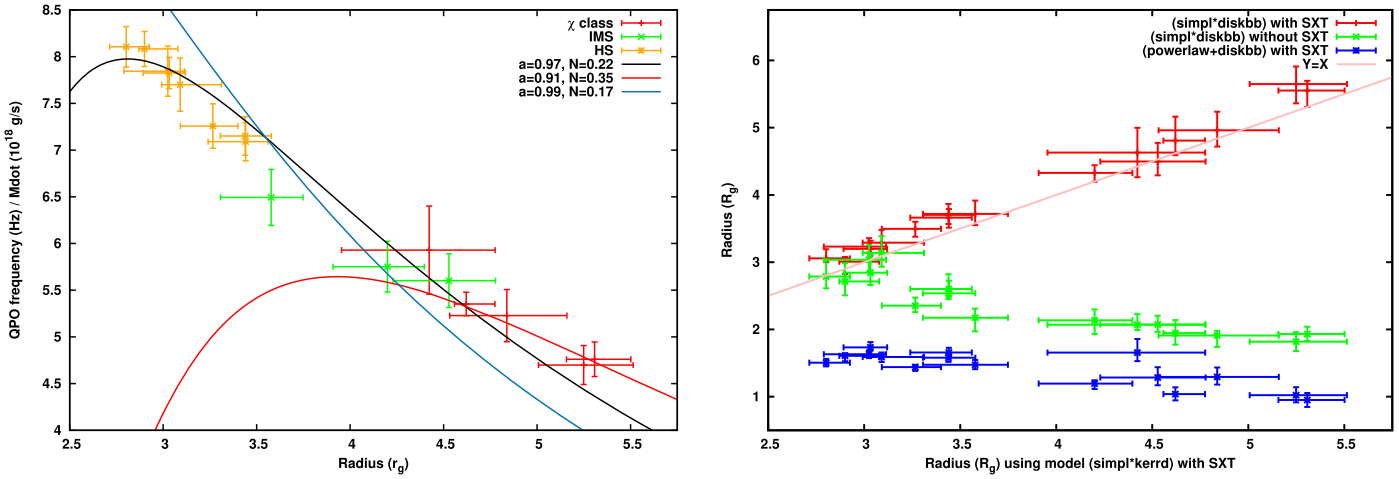

Figure 4. Left panel shows variation of QPO frequency divided by the accretion rate with inner disk radii. The lines represent the $\frac{f_{\rm dyn}}{\dot{M}_{18}}$ as predicted by the relativistic standard accretion disk model (Equation (3)) for dimensionless spin parameter $a = 0.973 \pm 0.002$ (best fit with $N = 0.22 \pm 0.01$ and reduced $\chi^2 \sim 0.5$), $a = 0.91$ ($N = 0.35$), and $a = 0.99$ ($N = 0.17$). In the right panel we show a comparison of the estimated values of the inner disk radii.

insignificant. Table 1 lists the best-fit values of the parameters, which are the accretion rate, inner disk radius, the fraction scattered into the Comptonizing medium, the index of the Comptonized spectrum, and flux in the line emission.

3. Results

The upper left panel of Figure 3 shows the variation of the QPO frequency with radius where a broad anticorrelation is visible; however, it is difficult to quantify the dependence because of the significant scatter. Indeed, the scatter suggests that the QPO frequency depends not only on the inner radius but also on some other parameter. The upper right and bottom panels of Figure 3 show the variation of the frequency with the accretion rate and the accretion rate with inner radii, where again there seems to be a correlation but with a large scatter. However, if one considers the frequency to depend both on the radius and the accretion rate and in particular if it is of the form $\propto \dot{M} F(R_{\rm in})$ then the correlation is significantly better. This is illustrated in the left panel of Figure 4 where the QPO frequency divided by the accretion rate is plotted against the inner radius. More pertinently the variation is the same as predicted by the standard accretion model for the dynamic frequency (Equation (3)) represented by lines for different values of the spin parameter a. Note that the predicted functional form depends only on a and the normalization factor N which should be of order unity. While a formal fit gives $a = 0.973 \pm 0.002$, we also show the variation for two different values of $a = .91$ and $a = .99$ to illustrate the constraints the data imposes on a.

It is interesting to note that the best-fit value of the black hole spin parameter obtained here is $a \sim 0.973 \pm 0.002$, which is consistent with $a = 0.98 \pm 0.01$ obtained independently by fitting the relativistically blurred reflection model to the broadband spectrum from *Suzaku* (Blum et al. 2009). While earlier results using *RXTE* and *Advanced Satellite for Cosmology and Astrophysics* (*ASCA*) spectra gave contradictory results (McClintock et al. 2006; Middleton et al. 2006), the better spectral resolution of *Suzaku* and the broadband analysis makes the results obtained by Blum et al. (2009) more reliable. We stress that the consistent determination of the spin parameter using two completely independent different methods significantly strengthens the interpretation present in this work.

We emphasis that the primary result used in this work, i.e., the estimate of the inner disk radii is not sensitive to the relativistic "kerrd" and "kerrdisk" models and they have been invoked for consistency. An alternate empirical model "*tbabs*(simpl*diskbb +Gaussian)*" provides nearly the same estimates of the inner radii as shown in the right panel of Figure 4 where the two radii estimates are compared. There are two primary reasons for obtaining a reliable value of the radii, which are (a) the presence of low-energy data from SXT and (b) the use of "simpl" to model the Comptonization instead of a power law. This is illustrated in the right panel of Figure 4, where the radii estimates without the SXT data (using the same empirical model ("*tbabs*(simpl*diskbb +Gaussian)*") are plotted against those obtained from the relativistic models with SXT. Without SXT data the radii estimated are systematically lower and not correlated with the ones obtained when SXT data are considered. The right panel of Figure 4 also shows the case, when a power-law model is used instead of "simpl" (with SXT data). In this case also the radii obtained are systematically underestimated and not well correlated with the values estimated when "simpl" is used.

During the HS, the overall flux and spectra evolve (Rawat et al. 2019), while here we have considered a time-averaged spectrum. To verify the impact of this on the results presented, we performed flux-resolved spectroscopy for all heartbeat observations by dividing the data into three flux levels and obtaining the corresponding spectra. We find that the qualitative nature as shown by the left panel of Figure 4 does not change with best-fit values $a = 0.968 \pm 0.002$ and $N = 0.24 \pm 0.01$ with reduced $\chi^2 \sim 1.1$, close to the ones obtained using time-averaged spectra.

4. Discussion and Summary

The result obtained in this Letter relies on the accuracy of some measured and theoretically estimated quantities. Future improvement on the estimate of these would refine the fitting presented here and can provide a robust value of the spin parameter. These include the uncertainties in (a) the estimated distance to the source, mass of the black hole, and the inclination

angle used; (b) the effective area and response of the LAXPC and SXT detectors; and (c) the theoretically estimated color factor, especially since this was done for a non-spinning black hole (Shimura & Takahara 1995). Note that most of these uncertainties are independent of each other and will give rise to a secular shift in the radii and accretion rate.

The analysis has been done by fixing the neutral column density value, nH at $4 \times 10^{22}\,\mathrm{cm}^{-2}$, as obtained by Blum et al. (2009) using *Suzaku* data. If we instead allow it to vary, its value ranges from 3.5×10^{22} to $4 \times 10^{22}\,\mathrm{cm}^{-2}$ for different orbits with a typical error of $0.1 \times 10^{22}\,\mathrm{cm}^{-2}$. Since we expect the column density not to vary during the course of the observation we have used the value obtained by Blum et al. (2009). If instead we use the average value obtained from the present observation, i.e., we fix it to $3.75 \times 10^{22}\,\mathrm{cm}^{-2}$, we get qualitatively similar results, with the best-fit values for the spin parameter and normalization being $a = 0.986 \pm 0.002$ and $N = 0.18 \pm 0.01$.

It is interesting to note that for small values of radius (i.e., $r \sim 4r_g$) the radial functional form of Equation (3) is approximately $1/r$ instead of $1/r^{2.5}$ due to its dependence on the relativistic terms A, B, D, E, and L. This means that the QPO frequency is roughly proportional to $\dot{M}/R_{\rm in}$, which in turn is proportional to the disk flux. Thus, an approximate dependence of the QPO frequency on total flux (if the disk component dominates) is expected in this scenario. Moreover, the spectral index of the Comptonization component may also depend on the disk flux, leading to a QPO frequency dependence on the index. For the spectral fitting results presented here, there is indeed a dependence of the spectral index on the disk flux, which will be physically interpreted in a later work where the evolution of the spectral parameters will be described in more detail. Here, we note, that in this interpretation dependence of QPO frequency on spectral index (Bhargava et al. 2019) is an indirect consequence of it being the dynamical frequency of a truncated disk as explicitly mentioned in Titarchuk & Osherovich (1999).

Since the QPO frequency depends both on the radius and accretion rate, this favors models based on hydrodynamics, especially, for example, the coronal oscillatory one (Titarchuk & Osherovich 1999; Titarchuk & Fiorito 2004; Shaposhnikov & Titarchuk 2007) where the frequency is indeed identified with the dynamic one. However, other models such as the accretion–ejection instability (Tagger & Pellat 1999; Varnière et al. 2002) are also promising, since evidence is provided for a driving instability. Although some of these theoretical models have a different identification of the QPO frequency, the result presented here now provides a strong foothold on which sophisticated models can be developed.

In summary, we exploit the broadband capability of *AstroSat* to study the spectral properties of GRS 1915+105 with the QPO frequency. We find that the frequency depends on the accretion rate and inner radius of the disk, just as was predicted for the dynamical frequency of a relativistic accretion disk. Thus, we identify the QPO frequency as the inverse of the sound cross time from the inner disk radius where strong General Relativistic effects dominate.

We thank the referee for constructive comments. This research has used the data of the *AstroSat* mission of the Indian Space Research Organisation (ISRO), archived at the Indian Space Science Data Centre. The authors would like to acknowledge the support from the LAXPC Payload Operation Center (POC) and SXT POC at the TIFR, Mumbai for providing support in data reduction.

References

Agrawal, P. C. 2017, JApA, 38, 27
Agrawal, P. C., Yadav, J. S., Antia, H. M., et al. 2017, JApA, 38, 30
Arnaud, K. A. 1996, in ASP Conf. Ser. 101, Astronomical Data Analysis Software and Systems V, ed. G. H. Jacoby & J. Barnes (San Francisco, CA: ASP), 17
Belloni, T., Psaltis, D., & van der Klis, M. 2002, ApJ, 572, 392
Bhargava, Y., Belloni, T., Bhattacharya, D., & Misra, R. 2019, MNRAS, 488, 720
Blum, J. L., Miller, J. M., Fabian, A. C., et al. 2009, ApJ, 706, 60
Brenneman, L. W., & Reynolds, C. S. 2006, ApJ, 652, 1028
Casella, P., Belloni, T., Homan, J., & Stella, L. 2004, A&A, 426, 587
Ebisawa, K., Życki, P., Kubota, A., Mizuno, T., & Watarai, K.-Y. 2003, ApJ, 597, 780
Homan, J., Wijnands, R., van der Klis, M., et al. 2001, ApJS, 132, 377
McClintock, J. E., Shafee, R., Narayan, R., et al. 2006, ApJ, 652, 518
Middleton, M., Done, C., Gierliński, M., & Davis, S. W. 2006, MNRAS, 373, 1004
Mikles, V. J., Varniere, P., Eikenberry, S. S., Rodriguez, J., & Rothstein, D. 2009, ApJL, 694, L132
Motta, S. E., Belloni, T. M., Stella, L., Muñoz-Darias, T., & Fender, R. 2014, MNRAS, 437, 2554
Muno, M. P., Morgan, E. H., & Remillard, R. A. 1999, ApJ, 527, 321
Narayan, R., & McClintock, J. E. 2008, NewAR, 51, 733
Novikov, I. D., & Thorne, K. S. 1973, in Black Holes (Les Astres Occlus), ed. C. DeWitt & B. DeWitt (New York: Gordon & Breach), 343
Psaltis, D., Belloni, T., & van der Klis, M. 1999, ApJ, 520, 262
Rawat, D., Pahari, M., Yadav, J. S., et al. 2019, ApJ, 870, 4
Reid, M. J., McClintock, J. E., Steiner, J. F., et al. 2014, ApJ, 796, 2
Remillard, R. A., Sobczak, G. J., Muno, M. P., & McClintock, J. E. 2002, ApJ, 564, 962
Shakura, N. I., & Sunyaev, R. A. 1973, A&A, 500, 33
Shapiro, S. L., Lightman, A. P., & Eardley, D. M. 1976, ApJ, 204, 187
Shaposhnikov, N., & Titarchuk, L. 2007, ApJ, 663, 445
Shimura, T., & Takahara, F. 1995, ApJ, 445, 780
Singh, K. P., Stewart, G. C., Chandra, S., et al. 2016, Proc. SPIE, 9905, 99051E
Singh, K. P., Stewart, G. C., Westergaard, N. J., et al. 2017, JApA, 38, 29
Sobczak, G. J., McClintock, J. E., Remillard, R. A., et al. 2000, ApJ, 531, 537
Steiner, J. F., Narayan, R., McClintock, J. E., & Ebisawa, K. 2009, PASP, 121, 1279
Stella, L., Vietri, M., & Morsink, S. 1999a, ApL&C, 38, 57
Stella, L., Vietri, M., & Morsink, S. M. 1999b, ApJL, 524, L63
Tagger, M., & Pellat, R. 1999, A&A, 349, 1003
Titarchuk, L., & Fiorito, R. 2004, ApJ, 612, 988
Titarchuk, L., & Osherovich, V. 1999, ApJL, 518, L95
van der Klis, M. 2005, AN, 326, 798
Varnière, P., Rodriguez, J., & Tagger, M. 2002, A&A, 387, 497
Wijnands, R., Homan, J., & van der Klis, M. 1999, ApJL, 526, L33
Wilms, J., Allen, A., & McCray, R. 2000, ApJ, 542, 914
Yadav, J. S., Agrawal, P. C., Antia, H. M., et al. 2016, Proc. SPIE, 9905, 99051D